a

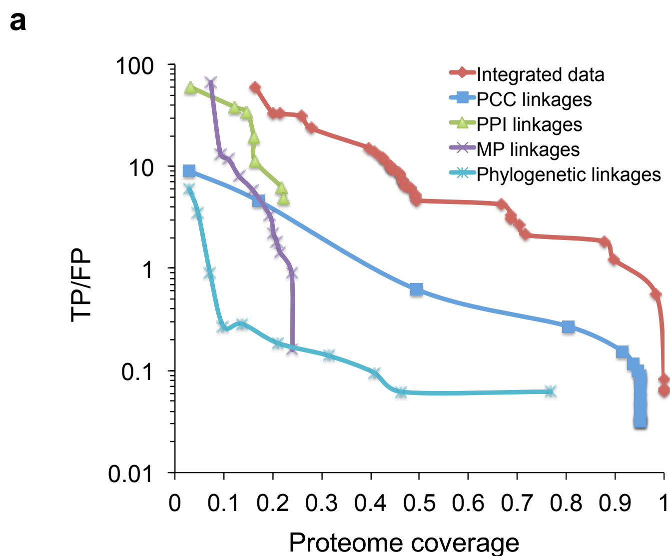

b

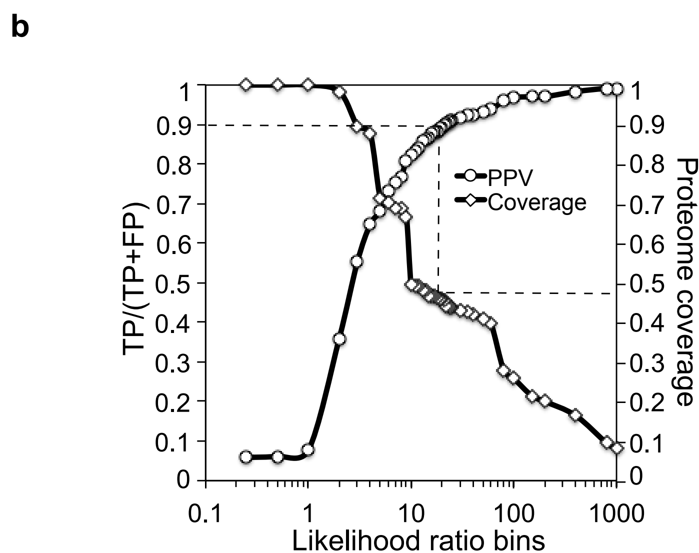

Fig. S1. The high-confident functional network of macrophage. **a**, The relationship between TP/FP ratio thresholds and proteome coverage of the individual input data set: Pearson correlation coefficiency (PCC) of microarray data, protein-protein interaction (PPI) and mutual information of gene phenotype (MP) and phylogenetic profiles, illustrates the contribution of each individual input to the integrated network data set. TP, true positive. FP, false positive. **b**, The predictive precision rates (TP/(TP+FP)) at different likelihood score cutoffs were evaluated by tenfold cross-validation and plotted against the proteome coverage. Each dot of the ratio represents an average of ten cross-validations at a particular likelihood score cutoff. The vertical dashed line shows the likelihood score cutoffs and proteome coverage corresponding to the predictive precision rate of 90% and likelihood score thresholds (LS) of 21. The ~90% confident network consists of 153,085 linkages with total 12775 genes as shown in Supplementary Table S4.

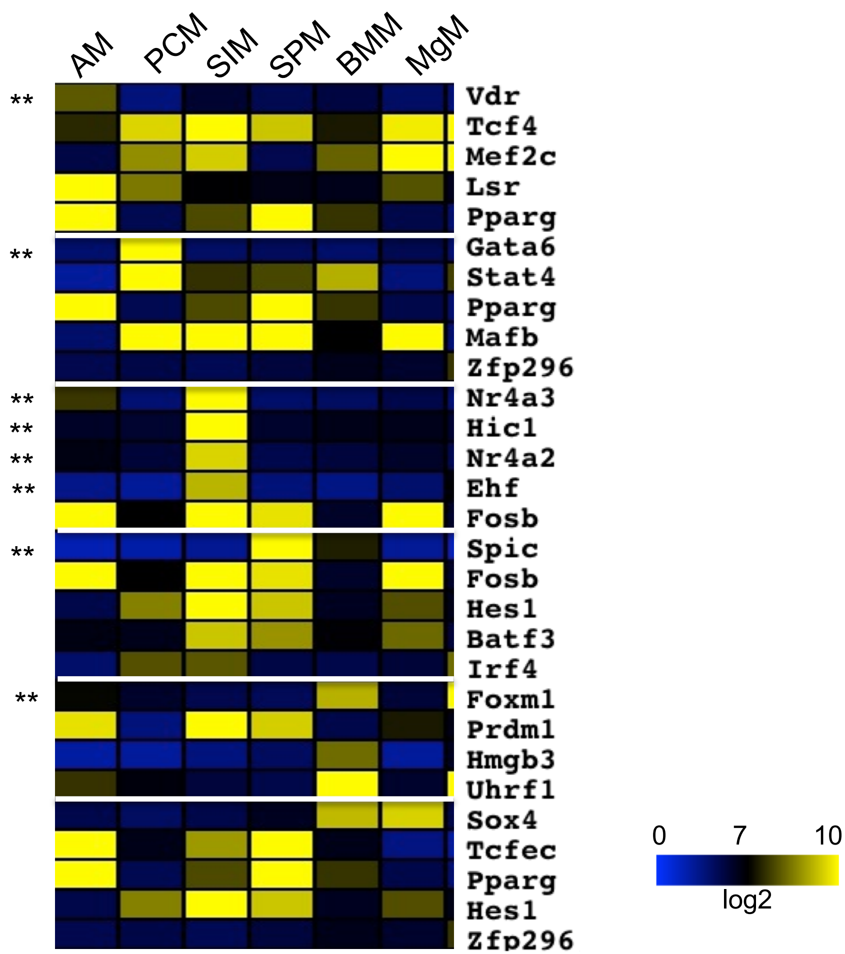

Fig. S2. Gene expression of identified key TFs based on public microarray data GSE15907. ** indicates the expressiion of tissue-specific TFs.

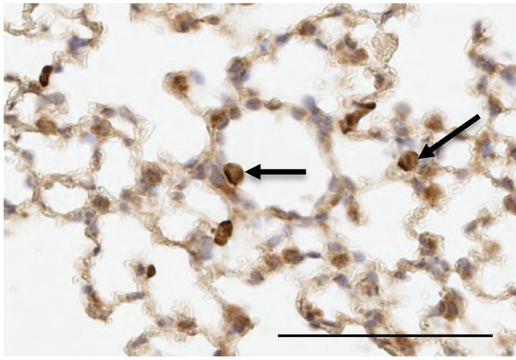

Fig. S3. Immunohistological staining of VDR in mouse lung. Arrows indicate alveolar macrophages. Scale bar: 100μM.

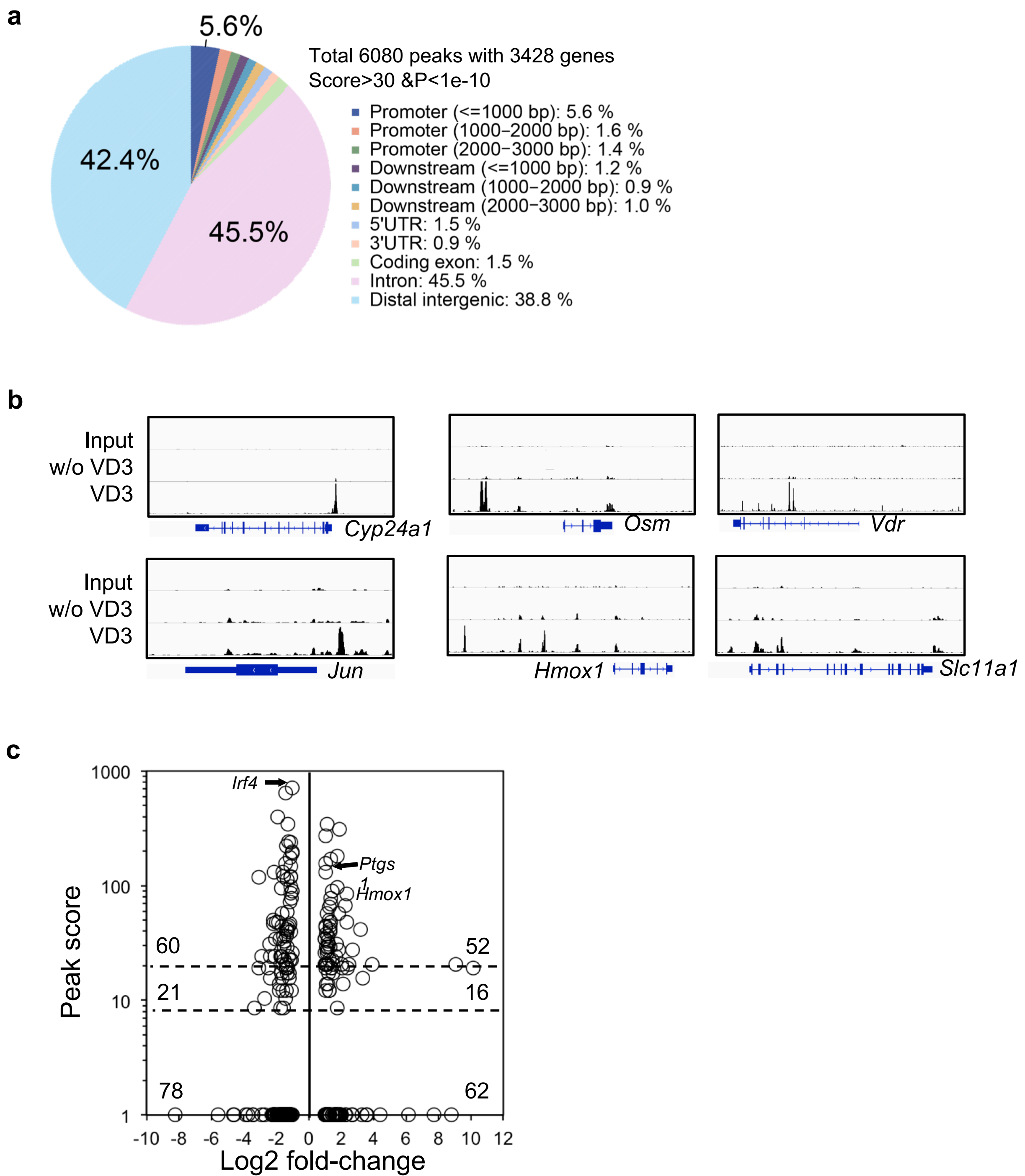

Fig. S4. ChIP-seq analysis of VDR in AM. **a**, Distribution of VDR-binding peaks calculated by MACS. **b**, Genome-browse of VDR-binding peaks of selected genes by IGV. **c**, Comparison of VDR-binding genes and all expression changed genes in *Vdr*$^{-/-}$ AMs.

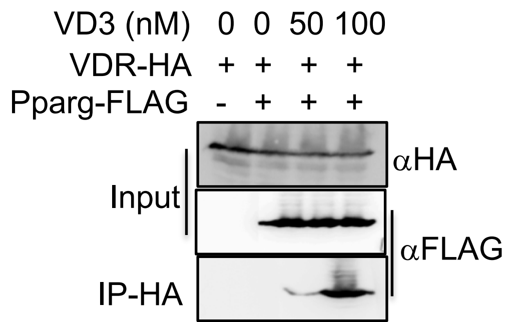

Fig. S5. Co-IP of VDR with PPARG. 293FT cells were transiently transfected with HA-tagged VDR and FLAG-tagged PPARG. Cell lysates were precipitated with anti-HA and in the presence of different amount of VD3, subjected to Western blotting with anti-HA and anti-FLAG antibodies. Input is the total cell lysate.

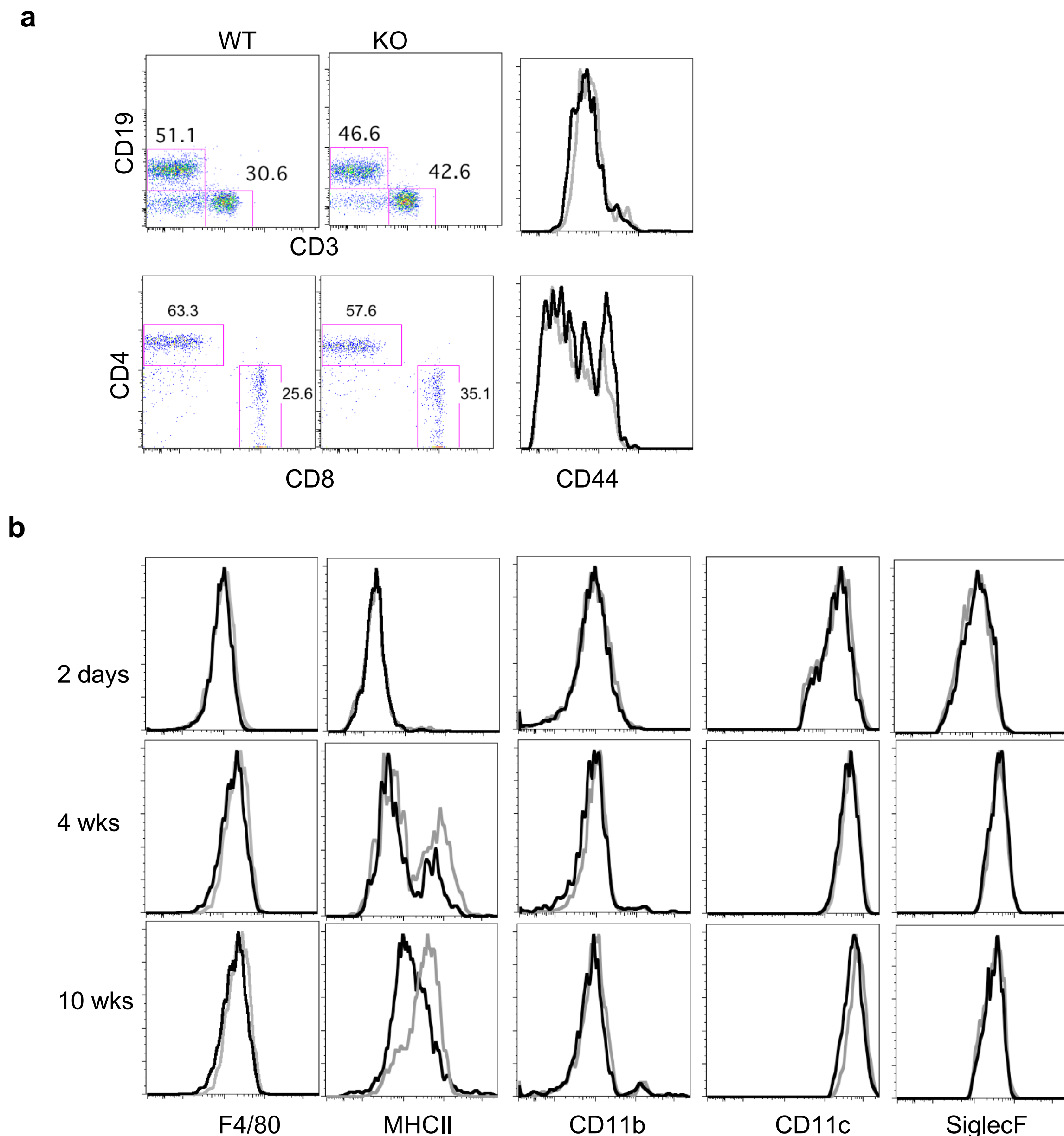

Fig. S6. Flow cytometry analysis of immune cells in mouse lungs of WT and *Vdr*$^{-/-}$ mice. **a**, Flow cytometry analysis of T and B cells from the lung tissues of WT and *Vdr*$^{-/-}$ littermates at 10 weeks of age. Single cell suspension was prepared by digesting the lung tissue and stained for CD45, CD19, CD3, CD4, CD8, NK1.1 and CD44. Shown are representative CD19 versus CD3 staining profiles gating on CD45^{+} cells, CD4 versus CD8 staining profiles gating on CD3^{+} cells. Histograms show CD44 expression by CD4 T cells (top) and CD8 T cells (bottom) from WT (black) and *Vdr*$^{-/-}$ (grey) mice. **b**, Expression of F4/80, MHCII, CD11b, CD11c and SiglecF in AM at different ages Cells from BAL were stained for CD45, F4/80, CD11c, CD11b, MHCII and SiglecF. Shown are representative histogram of expression of F4/80, MHCII, CD11b, CD11c and SiglecF in AM from in WT (black) and *Vdr*$^{-/-}$ mice (grey)(n=6 mice each per genotype and age group).

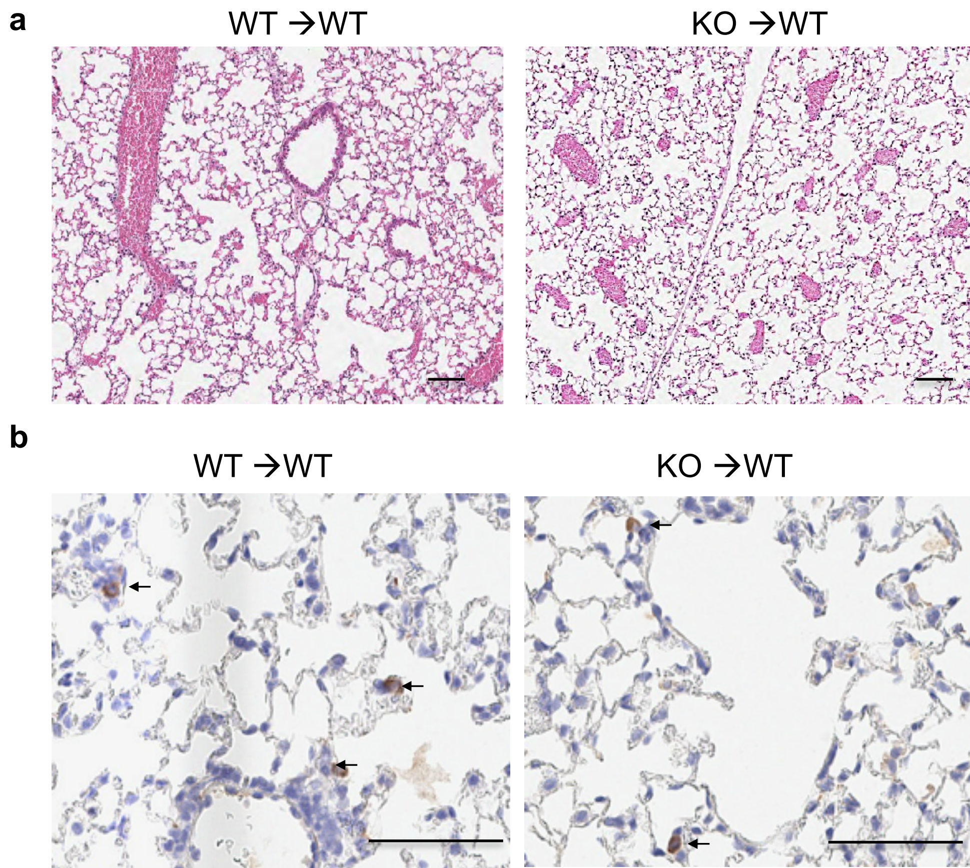

Fig. S7. Intratracheal transfer of *Vdr*$^{-/-}$ AM into WT B6 mice. **a**. H&E staining of lung section of adoptive once transfer mice. 1x10^{6} WT or *Vdr*$^{-/-}$ AM (CD45.2^{+}) were adoptively transferred into CD45.1^{+} B6 recipient mice. 6 weeks later, recipient mice were euthanized for H&E staining of lung sections. Shown are representative image from two independent experiments with total 4 mice per group. **b**, Anti-CD45.2 immunohistochemical staining of lung sections. 5x10^{5} WT or *Vdr*$^{-/-}$ AM (CD45.2^{+}) were adoptively transferred into CD45.1^{+} B6 recipient mice every week for four weeks (n=4 per group). 6 weeks after first transfer, recipient mice were euthanized for flow cytometry (Fig. 4g) or immunochemical statining (**b**) to confirm the presence of the transferred cells. Arrows point to CD45.2^{+} donor AM. Scale bars: 100μm.

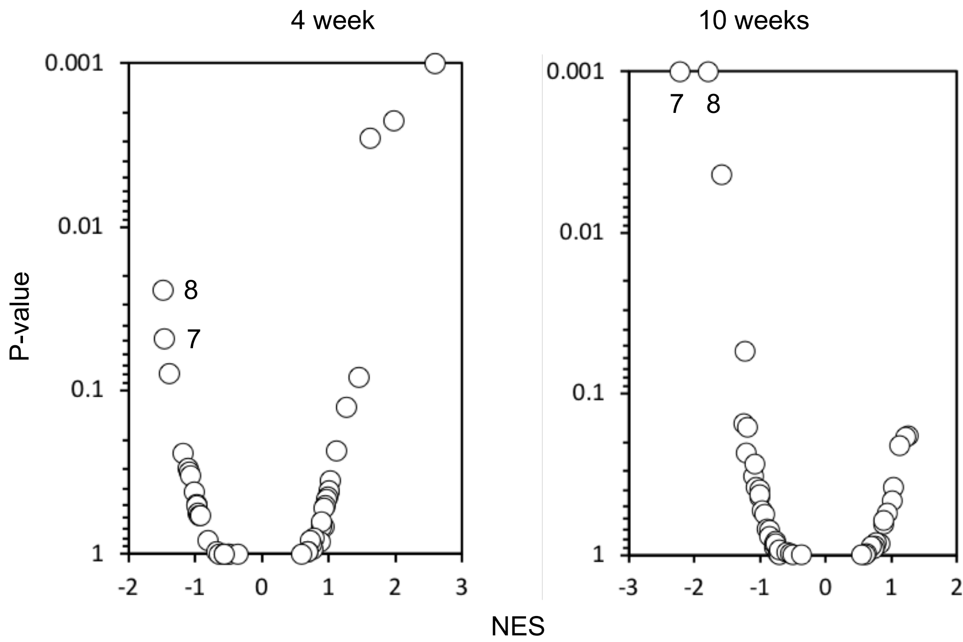

Fig. S8. Volcano plots of normalized enrichment scores (NES) and enrichment *P*-values of the gene sets of macrophage stimulation (Xue et al.) applied to expression data of *Vdr*$^{-/-}$ alveolar macrophages from mice at 4 and 10 weeks of age. Shown are representative results of several permutation runs of GSEA. Indicated module 8 and 7 is linked to IFNγ stimulation.

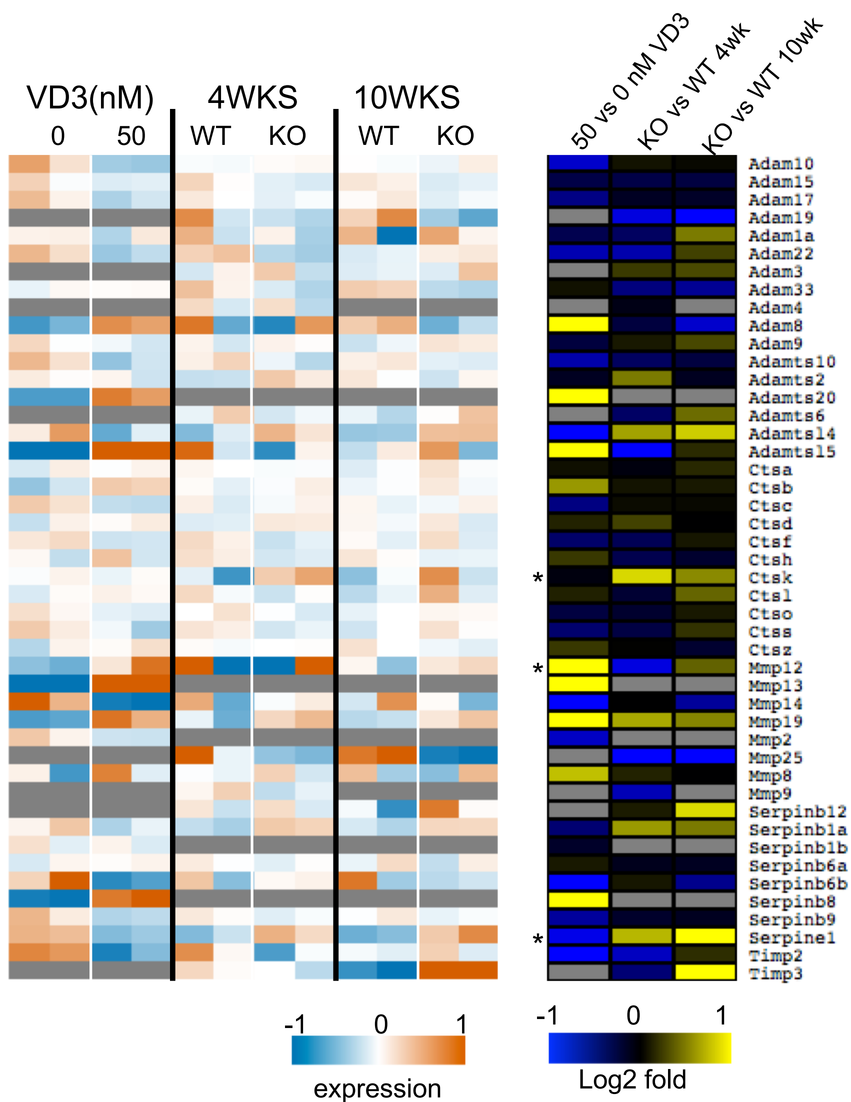

Fig. S9. Heatmap of gene expression (left panel) and fold-changes (right panel) of ECM-remodeling genes in AM induced by VD3 as well as in *Vdr*$^{-/-}$ AM as compared to WT AM from 4 and 10 weeks old mice. Shown are centralized CPM (counts per million reads) and log2 fold changes in left panel and right panel, respectively. * indicates significant expression changes of several COPD disease genes .

a

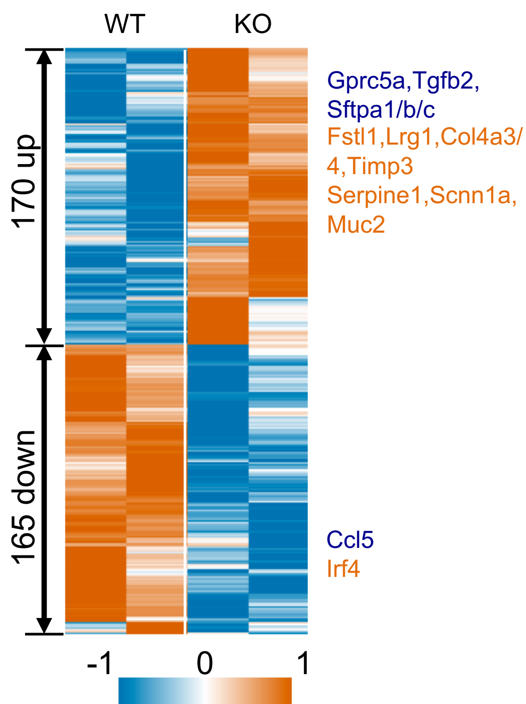

b

Functional Terms	#Genes	*P-Value*
Up-regulated:		
GO:0016477~cell migration	27	6.2E-07
GO:0007155~cell adhesion	29	7.6E-07
GO:0007166~cell surface receptor signaling	34	9.2E-05
GO:0042127~regulation of cell proliferation	26	0.00022
GO:0042060~wound healing	11	0.00029
Down-regulated:		
GO:0006955~immune response	43	8.6E-18
GO:0006952~defense response	38	5.9E-12
GO:0002253~activation of immune response	19	1.9E-11
GO:0045087~innate immune response	23	7.6E-10
GO:0045321~leukocyte activation	25	8.5E-09
GO:0001816~cytokine production	20	2.6E-07

Fig. S10. Expression changes in *Vdr*$^{-/-}$ AM as compared to WT AMs from 10 weeks old mice. **a**, Heatmap of gene expression of 170 up-regulated and 165 down-regulated genes in *Vdr*$^{-/-}$ AM as compared to WT AMs from 10 weeks old mice. Shown is centralized CPM (counts per million reads). **b**, GO enrichment analysis showing enrichment of certain pathways in the up-regulated and down-regulated genes. GO sets of biological process, number of genes and P-value are shown.

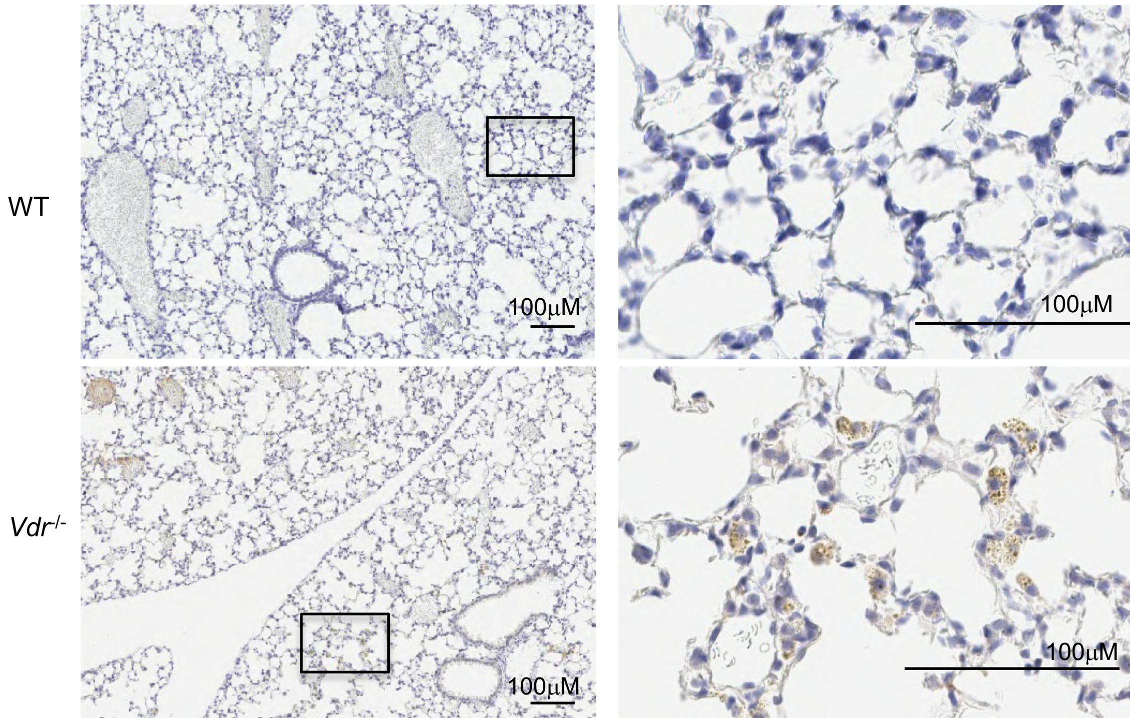

Fig. S11. ROS-induced DNA damage in lungs of *Vdr*$^{-/-}$ mice. Shown are representative anti-8OHdG immunohistochemical staining of lung sections of WT and *Vdr*$^{-/-}$ mice (3 mice per group).

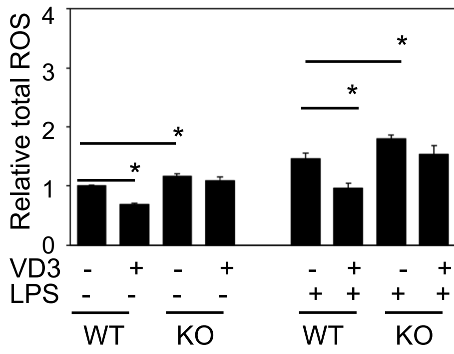

Fig. S12. Comparison of ROS levels in WT and *Vdr*$^{-/-}$ AM. WT and *Vdr*$^{-/-}$ AM were cultured for 1 hr in the absence or presence LPS and/or VD3. Intracellular ROS level was detected by CM-H2DCFDA and flow cytometry. Data are from three independent experiments. Statistical significance is calculated by T-test. * $P<0.05$.